

Laboratory of Biomedical Engineering
Department of Engineering Physics and Mathematics
Helsinki University of Technology
Espoo, Finland

Methodological Aspects for Improving Clinical Value of SPECT and MRI

Outi Sipilä

Espoo 2000

Laboratory of Biomedical Engineering
Department of Engineering Physics and Mathematics
Helsinki University of Technology
Espoo, Finland

Methodological Aspects for Improving Clinical Value of SPECT and MRI

Outi Sipilä

Dissertation for the degree of Doctor of Technology to be presented with due permission for public examination and debate in Auditorium F1 at Helsinki University of Technology (Espoo, Finland) on the 26th of April, 2000, at 12 o'clock noon.

Espoo 2000

ISBN 951-22-4958-8

Preface

This thesis has been completed while I have been working in the Laboratory of Biomedical Engineering, Helsinki University of Technology, and in various departments of Helsinki University Central Hospital (currently Health Care Region of Helsinki and Uusimaa). I have been a student in graduate school “Functional Research in Medicine”. I am deeply grateful to my supervisor, Professor Toivo Katila, for the support during my studies and excellent working conditions in the Laboratory of Biomedical Engineering. I would also like to thank Professor Kristian Liewendahl, Professor Carl-Gustav Standertskjöld-Nordenstam and Professor Pekka Karp for the opportunity to do research work in hospital environment.

I wish to express my gratitude to my instructor, Professor Ari Visa, for the advice and discussions during the long years of work. I have also appreciated the general discussions about Life, especially during difficult periods. My other instructor, Docent Sauli Savolainen, deserves warm thanks for his professional guidance as well as practical suggestions for everyday life in the hospital.

My closest collaborators have been Päivi Nikkinen, Ph.D., and Hanna Pohjonen, Dr. Tech., whose support and friendship I have enjoyed. I have also had the pleasure to work with Professor Kristian Liewendahl, whose expertise has been crucial with the publications related to SPECT. I am deeply grateful to Docent Oili Salonen for her invaluable help and never-ending patience in analyzing MR images. The assistance of Veli-Pekka Poutanen, Lic. Phil., in MR imaging and image transfer is gratefully acknowledged, as well as the collaboration of two specialists in epilepsy, Docent Marja-Liisa Granström and Eija Gaily, M.D. I am also grateful for the contribution of the other co-authors of the publications. I wish to thank Docent Timo Erkinjuntti for the opportunity to work with the images of the SAM project.

I truly appreciate the help and patience of the personnel of the Division of Nuclear Medicine, Laboratory Department, and Epilepsy Unit, Hospital for Children and Adolescents, as well as Department of Radiology, Helsinki University Central Hospital. I am also grateful to the staff of the Laboratory of Biomedical Engineering for the good working atmosphere and practical help. Besides scientific collaboration, Jyrki Lötjönen, M.Sc. (Eng.), deserves special thanks for taking care and informing me of many practical things related to this dissertation process.

I wish to thank Docent Matti Koskinen and Professor Hannu Eskola for the constructive criticism and suggestions on the manuscript.

Financial support from the Academy of Finland, Finnish Society of Nuclear Medicine and the Jenny and Antti Wihuri Foundation is gratefully acknowledged.

My dear husband Seppo has been persistently taking care of my welfare, although I have not always been very receptive during this work. Thank you, Seppo, for your loving encouragement and the many laughs even in the darkest days.

Espoo, March 2000

Outi Sipilä

Contents

List of publications	ii
List of abbreviations	iii
1 INTRODUCTION	1
2 SPECT	4
2.1 Segmentation	5
2.2 Transmission imaging	6
3 BRAIN MRI	10
3.1 Preprocessing	10
3.2 Segmentation	11
3.2.1 Statistical and neural network classification	11
3.2.2 Evaluation of segmentation results	16
4 MULTIMODAL APPROACHES	17
4.1 Brain SPECT and MRI	18
4.2 Registration error	18
4.3 Transmission imaging for registration	20
5 CONCLUSIONS	23
6 SUMMARY OF PUBLICATIONS	26
References	28

List of publications

This thesis consists of an overview and of the following six publications:

- I S. Savolainen, H. Pohjonen, O. Sipilä, K. Liewendahl. Evaluation of segmentation methods for volume determination in In-111/Tc-99m SPET. *Nucl Med Commun*, 16:370-377, 1995.
- II A. Stocker, O. Sipilä, A. Visa, O. Salonen, T. Katila. Stability study of some neural networks applied to tissue characterization of brain magnetic resonance images. In *Proceedings of the IAPR 13th International Conference on Pattern Recognition, Vol. IV*, 472-477, 1997.
- III O. Sipilä, A. Visa, O. Salonen, T. Erkinjuntti, T. Katila. Experiences on data quality in automatic tissue classification. *Report TKK-F-A794, Helsinki University of Technology*, 1999.
- IV H. Pohjonen, P. Nikkinen, O. Sipilä, J. Launes, E. Salli, P. Karp, J. Ylä-Jääski, T. Katila, K. Liewendahl. Registration and display of brain SPECT and MRI using external markers. *Neuroradiology*, 38:108-114, 1996.
- V O. Sipilä, P. Nikkinen, H. Pohjonen, V.-P. Poutanen, A. Visa, S. Savolainen, T. Katila, K. Liewendahl. Accuracy of a registration procedure for brain SPET and MRI: phantom and simulation studies. *Nucl Med Commun*, 18:517-526, 1997.
- VI O. Sipilä, P. Nikkinen, S. Savolainen, M.-L. Granström, E. Gaily, V.-P. Poutanen, H. Pohjonen, K. Liewendahl. Transmission imaging for registration of ictal and interictal single-photon emission tomography, magnetic resonance imaging and electroencephalography. *Eur J Nucl Med*, 27:202-205, 2000.

Statement of involvement

All publications included in this thesis are a result of a group effort. In Publ. I, the author of this thesis implemented and documented the segmentation algorithms utilized. In Publ. II, the author took actively part in preprocessing the images, analyzing the results and writing the publication. Publ. III consists mainly of the work done by the author of this thesis. In Publ. IV, the author of this thesis implemented the segmentation utilities and took part in implementation of the registration protocol and writing the publication. The phantom measurements and simulations in Publ. V as well as the registration protocol and phantom measurement of Publ. VI were designed and implemented by the author. The filling and imaging of the phantoms were done in collaboration with the physicists of the group. The software in Pubs. V and VI was implemented by the author, except the Borgefors' algorithm. Pubs. III, V and VI were written by the author of this thesis.

List of abbreviations

2D	two-dimensional
3D	three-dimensional
3-NN	three nearest neighbours
5-NN	five nearest neighbours
CT	X-ray computed tomography
DMSA	dimercaptosuccinic acid
ECD	ethyl cysteinate dimer
EEG	electroencephalography
FBP	filtered backprojection
FWHM	full width at half maximum
GL	gray level histogram or adaptive thresholding
GM	gray matter
HSE	herpes simplex encephalitis
HMPAO	hexamethylpropylene amine oxime
HUCH	Helsinki University Central Hospital
k-NN	k nearest neighbours
LEGP	low energy general purpose
LEUHR-PAR	low energy ultra high resolution parallel
LVQ	learning vector quantization
ML-EM	maximum likelihood expectation maximization
MEG	magnetoencephalography
MRI	magnetic resonance imaging
NMR	nuclear magnetic resonance
OS-EM	ordered subsets expectation maximization
PDw	proton density weighted
PET	positron emission tomography
PVE	partial volume effect
rCBF	regional cerebral blood flow
RF	radio frequency
RMS	root-mean-squared
ROI	region of interest
SAM	Helsinki Stroke Aging Memory (research study)
SD	standard deviation
SNR	signal-to-noise ratio
SOM	self-organizing map
SPECT (SPET)	single photon computed emission tomography
T1w	T1 weighted
T2w	T2 weighted
VOI	volume of interest
WM	white matter

1 INTRODUCTION

Modern medical imaging modalities produce three-dimensional (3D) digital information from inside the human body without invasive operations. Imaging examinations belong to widely used diagnostic procedures. Development of fast computers enables new applications, continuously growing the amount of image data produced in hospitals. Efficient use of imaging requires powerful means to extract the information from the large amount of data. Image processing is a growing field of research interest in medical as well as in other applications. In medical imaging, the reliability of imaging as well as of further processed results is of uttermost importance.

Emission tomography is based on measuring the distribution of a radiopharmaceutical administered to a patient. To provide information on a physiological function, the radiopharmaceutical, usually consisting of the radionuclide and the bounding compound, should model but not affect the system under study [1]. Isotopes used in single photon emission computed tomography (SPECT) decay emitting photons, which are detected and used to form the image. The half life of the isotope is usually several hours or even days.

SPECT is utilized for a large variety of applications, including oncological and cardiac studies, inflammatory diseases, study of kidney function and cerebral diseases. Study of regional cerebral blood flow (rCBF) has diagnostic value e.g. in patients with epilepsy [2], cerebral infarction [3] and herpes simplex encephalitis (HSE) [4]. Tracers utilized in imaging rCBF include ^{99m}Tc -hexamethylpropylene amine oxime (^{99m}Tc -HMPAO) and ^{99m}Tc -ethyl cysteinate dimer (^{99m}Tc -ECD). They have a high first-pass brain extraction rate, and the maximum uptake is achieved in 30-60 s from injection [5]. After that, the cerebral perfusion pattern is stable for several hours allowing imaging immediately or at a later time, e.g. when an epileptic seizure is over [2]. Most studies are evaluated visually by a physician. Semiquantitative analysis of brain perfusion SPECT images can be based on regions of interest (ROIs), which are compared to each other or normalized to cerebellar or whole brain mean counts for comparison to age-dependent normal databases. Dopamine transporter and receptor studies are utilized e.g. for patients with Parkinson disease or schizophrenia. Quantification of the specific binding of the radiopharmaceutical is often computed as striatum to cerebellum, striatum to frontal lobe or caudatus to putamen ratio based on operator drawn ROIs [6].

In epileptic patients, interictal imaging alone is not reliable [2]. In an ictal study, the tracer is injected as soon after the seizure onset as possible to detect the primary epileptic zone. According to the results of Zubal et al. [7] with ^{99m}Tc -HMPAO, injecting immediately after the seizure onset is optimal, since hyperperfusion is detected in the area of seizure onset. In a later time, there may be no detectable differences in rCBF since the rCBF

in an epileptic region is in transition from hyper- to hypoperfusion. Injection during the evolution of the seizure may show as well hypo- as hyperperfusion regions. In this case, the primary epileptogenic region may already be seen as a hypoperfusion area and the distribution pattern of the seizure as a hyperperfusion area. Video-electroencephalography (video-EEG) monitoring is necessary when injecting for ictal and interictal SPECT in order to verify the state of the patient.

Several aspects lower the quality of information from SPECT. The images are degraded by several imaging errors including radiation attenuation and scatter, which makes quantitative analysis difficult. Manual drawing of ROIs makes the analysis subjective when compared to automatic segmentation methods. Although functional defects can be detected with SPECT, the localization of the defects is more difficult due to the modest resolution of SPECT. Anatomical details can be obtained from X-ray computed tomography (CT) or from magnetic resonance imaging (MRI).

MRI is based on the phenomenon of nuclear magnetic resonance (NMR) [8]. Nuclei with an odd number of nucleons, exposed to a uniform static magnetic field, can be excited with a radio frequency (RF) pulse with the proper frequency and energy [1]. After the excitation pulse, an NMR signal can be recorded. The return to equilibrium is characterized by relaxation times T_1 and T_2 , which depend on the nuclei imaged and on the molecular environment. Mainly hydrogen nuclei (protons) are imaged in clinical applications of MRI, because they are the most NMR-sensitive nuclei and have the largest physiological concentration among biologically important nuclei in the human body [8]. In Fourier imaging techniques, the image is reconstructed from the measured data using Fourier transformation [1, 9]. Selection of the pulse sequence and the imaging parameters affects contrast between tissue types in the images. As an added advantage when comparing to other imaging modalities, spatially matched multispectral information can be obtained using different acquisition parameters.

Besides its other applications, MRI is one of the basic neurological examinations. Although more expensive than CT and with limited availability, MRI has superior contrast between soft tissues in the brain when compared to CT. Since the patient is not exposed to ionizing radiation, patient safety does not limit the obtainable resolution and there are usually no ethical problems with imaging volunteers for scientific purposes. Besides visual examination in every day clinical practise, computer assisted analysis of MR images has been under major research interest. Because MRI produces accurate anatomical information, segmentation of MR images allows 3D visualization and quantitative analysis. Clinical application areas include 3D surgery planning and simulation, 3D radiation treatment planning and follow-up of tumour response during therapy, and follow-up of brain tissue volumes in neurodegenerative diseases such as multiple sclerosis [10, 11, 12, 13, 14]. Extraction of intra- as well

as extracranial tissue boundaries, e.g. for source localization in magnetoencephalography (MEG) or EEG, is also an important application (e.g. [15]). Factors that may degrade image quality and complicate computer assisted analysis include geometrical distortions, noise and intensity nonuniformity (i.e. intensity values vary with the location in the image).

In computer assisted analysis of medical images, the most difficult operation is usually segmentation of the data. Segmentation means extraction of objects of interest from the image. The object can be an organ such as the brain or a specific type of tissue such as the white matter in the brain. In this work, the term segmentation includes both grouping of the volume elements (voxels) of the image to larger regions and labelling of meaningful entities constructed from the grouped voxels. Manual segmentation is usually too time-consuming for clinical practice since the image can consist of tens or even hundreds of slices. General and at the same time automatic methods have not been invented. Fortunately, the processing time can be considerably lowered with semi-automatic methods. As the quality of the analysis following segmentation depends on the accuracy of the segmentation result, the evaluation of the segmentation method is very important. Inherent error present in segmentation results is due to the fact that the image is formed of discrete voxels leading to the partial volume effect (PVE), i.e. a voxel may contain signal from several tissue types.

Image registration is utilized to achieve spatially correlated information from different imaging modalities, enabling voxel-by-voxel comparison of images with complementary information. Registration of digital images is never perfect due to the discrete nature of the voxels. Other error sources are usually also present. However, the registration error should not be the limiting factor in the analysis of the registered images in order the registration to be useful.

The aim of this thesis was to improve clinical value obtained from SPECT and MRI by developing data processing methods and validating their usefulness, accuracy and reliability in clinical environment. More specifically, the clinical challenges included 1) improvement in the reliability of ROI analysis of SPECT images, 2) gathering tissue boundary and volumetric information from brain MRI and validating the reliability of the process, and 3) improvement in localization of epileptogenic foci in epilepsy surgery candidates.

2 SPECT

Modern SPECT devices are usually based on the use of a rotating gamma camera [16]. The detector head(s) travel around the patient and register the emitted photons in a preselected accuracy. Collimation ensures that photons incident in the prescribed direction only arrive to the detector. Due to collimation, the sensitivity of SPECT is quite poor: only one photon per thousand is usually registered [17]. The image is reconstructed from the measured line projections. The most common reconstruction method in clinical use is filtered backprojection (FBP) [18]. Iterative methods [19, 20] have become a useful clinical option due to the rapid development of computers. The advantage of iterative methods is that known distortions during acquisition can be modelled and included in the projections and compensated during the reconstruction [21].

Quantitative analysis of SPECT images is usually directed to measuring activity ratios and object sizes [21]. Image quality is mainly determined by resolution, contrast (including sensitivity and noise) and activity administered to the patient (total counts during imaging) resulting in an optimization problem. When imaging objects that are small compared to the system resolution, increased resolution improves image quality more than does a large increase in counts [22]. However, the optimal compromise between resolution and sensitivity will depend on the total available photons [23]. Besides the intrinsic resolution of detectors, factors affecting the resolution of a SPECT system are collimator characteristics [21, 23, 24, 25], spatial and angular sampling [21, 26], acquisition mode [21], and reconstruction method [19, 25]. For example, the intrinsic resolution (full width at half maximum, FWHM) of Picker SX300 and Picker Prism 3000XP gamma cameras, utilized in this thesis, was 3.9-4.5 mm and 2.8-3.5 mm [6], respectively. The collimator dependent system resolution at 10 cm in air (FWHM) was 8.0-8.6 mm (low energy general purpose, LEGP, collimator) and 6.7 mm (low energy ultra high resolution parallel, LEUHR-PAR, collimator) for these cameras, respectively [6]. Filtering in connection with reconstruction is often a severe problem as the cutoff frequency imposes a difficult trade-off between correct voxel intensity and resolution [21, 27].

The most important physical factor affecting the quality of SPECT is photon attenuation [21, 25]. Primary photons are lost by photoelectric absorption or by scattering in the patient, resulting in image artefacts and inaccuracies in quantification [25]. Attenuation correction methods can be based on the assumption of uniform attenuation inside the patient [21, 25]. In more accurate methods, attenuation coefficient distribution is modelled through experimental measurements and included in iterative reconstruction of the image [25]. Transmission imaging enables the most accurate methods for attenuation correction [28]. Another major factor degrading visual image analysis and quantitative accuracy is the detection of scattered

photons [21, 25, 29, 30]. If scatter is coherent, the photon will be undistinguishable from primary non-scattered photons. Even Compton scattered photons are often confused with primary photons [25]. Scatter correction methods include different windowing techniques of the recorded energy spectrum limiting the detection of scattered photons [30], as well as compensation methods for the effects of recorded scattered photons such as filtering and convolution methods [29, 30].

2.1 Segmentation

In order to enhance quantification of SPECT images, accurate delineation of the objects is desirable. If segmentation can be accomplished (semi)automatically, the analysis is more objective than with manual methods. Because the nature of SPECT images is functional and there are several imperfections in imaging, reliability of segmentation, manual or automatic, should be carefully checked with phantom experiments or simulations. Besides imaging imperfections, the segmentation method can introduce additional errors in quantification [31].

Thresholding is the most common approach in segmenting SPECT images [31, 32, 33, 34, 35]. Fixed thresholding is problematic since the correct threshold depends on factors such as size and contrast [31]. In patient images, neither the size of an object nor the activity vs. background activity is known beforehand preventing the utilization of phantom measurements to decide the correct threshold value. An automatic threshold selection method (adaptive thresholding, gray level histogram method, GL) has been adopted in some studies [31, 32]. Mortelmans et al. have proposed a least squares linear regression analysis between the actual and the estimated volumes in order to correct the systematic error from the adaptive thresholding [31]. This means vast amount of phantom experiments for different systems in different conditions. In Ref. [35], attenuation and scatter correction based on CT images was applied before segmentation with the adaptive thresholding. Also a context sensitive thresholding method using empirical rules has been developed [36]. Another approach for segmentation has been edge detection [32, 37]. Fuzzy c-means clustering has been utilized in classification of dynamic images investigating striatal dopamine receptor and serotonin transporter bindings [38]. The results from these publications are difficult to compare since there are significant differences in imaging protocols, phantoms and simulations utilized.

In Publ. I, fixed thresholding, adaptive thresholding (GL), region growing and a method combining region growing and edge detection were tested on phantom and patient images using ^{99m}Tc and ^{111}In . The methods as well as the imaging and reconstruction parameters have been introduced in the publication. Plain edge detection was not tested in this work. A correlation of 0.72 - 0.95 was detected between the true and measured phantom volumes with

the four methods. None of the tested methods produced optimal results to be generalized in the use with patient images. When comparing Publ. I and the work of Alaamer et al. [35], there were two differences in using the GL method, which may have had an impact on the poor results obtained with GL in Publ. I. First, nonuniform attenuation and scatter correction were not available in Publ. I. Second, one threshold was used for the whole image trying to extract two objects with it. In [35], a volume of interest (VOI) was first defined including only one object and background. In Ref. [39], a practical method for irregular VOI detection based on orthogonal maximum intensity projections was presented.

In Ref. [40], fixed thresholding was further analysed in order to achieve quantitative information from renal ^{99m}Tc -dimercaptosuccinic acid (DMSA) SPECT. The phantom consisted of an elliptical cylinder including two cylinders or spheres with volumes of 54-220 ml simulating the kidneys. Activity concentration in the objects was 159-337 MBq/l. Background concentration was 0.5-9.8 %. The phantom was imaged using Picker Prism 2000 2-head and Picker 3000XP 3-head cameras. The images were prefiltered using Butterworth lowpass, Wiener and Metz filters and reconstructed using FBP with a ramp filter [41]. Before thresholding, background was estimated as the mean value of voxels in a 5x5 window and subtracted from the image. Uniform attenuation correction [41] improved the detected activity ratio of the objects. Segmentation still remained a problem: thresholds which produced correct volumes and activity ratios depended on filtering and on the total activity of the object (Fig. 1). With the regularly shaped objects utilized in this phantom experiment, the slice thickness, camera and collimator, and background activity did not seem to have an impact on the correct thresholds.

2.2 Transmission imaging

The main application area of transmission imaging in SPECT is nonuniform attenuation correction. Besides that, transmission information can be utilized for scatter correction, movement analysis and registration [28, 42]. Opposed to positron emission tomography (PET), attenuation correction in SPECT is only an approximative correction [28]. In transmission imaging, the patient is exposed to an external radiation source and the transmitted radiation is measured. The attenuated (N_x) and nonattenuated (N_0) count rates are related by

$$N_x = N_0 e^{-\int \mu(x) dx}, \quad (1)$$

where μ is the linear attenuation coefficient depending on photon energy and electron density of the material [28]. For any projection, Eq. 1 gives the integral of attenuation coefficients:

$$\int \mu(x) dx = \ln \frac{N_0}{N_x}, \quad (2)$$

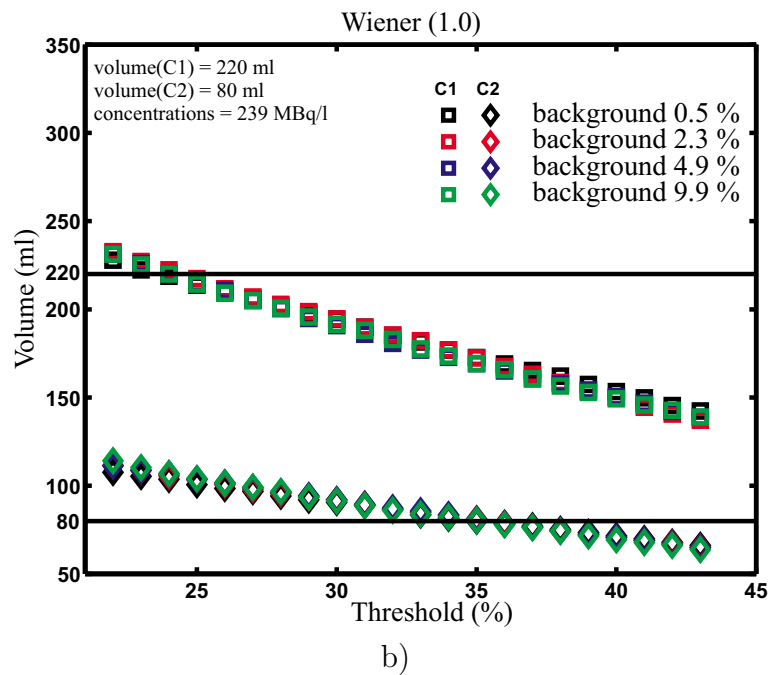
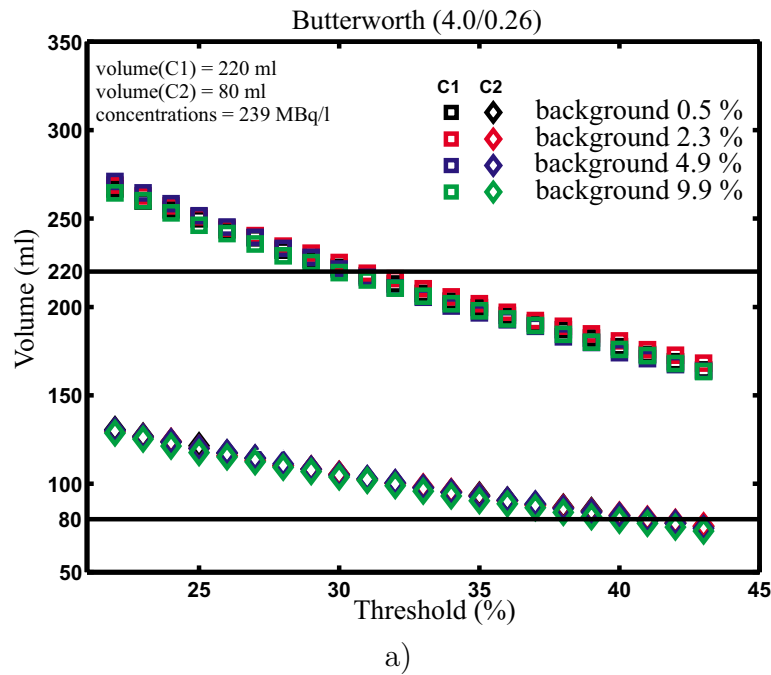


Fig. 1: Object volumes as a function of the fixed threshold used for segmentation. The thresholds are given as percentages of the maximum intensity value in the image. Thresholds producing correct volumes depended on filtering and activities. The camera was Picker Prism 3000XP with a LEUHR-PAR collimator and voxel size was $3.2 \times 3.2 \times 9.3 \text{ mm}^3$. In Fig. a) the prefilter was Butterworth filter (4.0/0.26) and in Fig. b) Wiener filter (1.0). Otherwise the reconstruction protocol was similar in both figures. Activity ratio of the objects (C1/C2) varied between 2.0 and 2.2 when using the same threshold value for both objects. The correct ratio was 2.8.

where N_0 is given by the count rate in a blank scan and N_x by the count rate in the transmission image. The transmission image can be reconstructed from the measured projections using FBP or iterative methods.

The emission count rate along any projection can be formulated as

$$C_x = \int C_0(x)(e^{-\int \mu(x_1)dx_1})dx, \quad (3)$$

where C_x is the integrated count rate from each attenuated point source $C_0(x)$ [28]. As the attenuation coefficient term cannot be separated from the emission count rate, attenuation correction must be approximated e.g. during the iterative reconstruction process using the attenuation coefficients measured with transmission imaging.

Simultaneous transmission and emission imaging have the advantage of reducing the scanning time and patient movement when compared to separate transmission and emission scans [43]. In the triple head Picker Prism 3000XP gamma camera utilized in this thesis, a simultaneous transmission imaging protocol [44, 45] was available using ^{153}Gd as the transmission line source. The transmission and emission raw data were first corrected for crosstalk. The transmission data was reconstructed using iterative maximum likelihood expectation maximization (ML-EM) reconstruction. This energy corrected attenuation map was utilized in the iterative ML-EM (or in the newer software version ordered subsets expectation maximization, OS-EM) reconstruction to correct attenuation. Also, scatter correction was enabled by measuring the scatter in two 4 keV windows one FWHM below and above the emission photopeak centerline and including this scatter image in reconstruction [45].

Besides utilizing transmission imaging in registration (c.f. Section 4.3), transmission based attenuation correction could have an impact on ROI based quantification of deep brain structures, such as basal ganglia. In Ref. [46], a cylindrical phantom ($d = 21.5$ cm, $h = 19$ cm) containing 10 kBq/ml Tc-99m was utilized to study the impact. Inside the cylinder, two spheres ($d = 4$ cm) were inserted with sphere/background activity ratios of 9.2 and 4.5. Alderson striatal phantom was also imaged using the striatum/background activity ratios of 3.0 and 2.0. In imaging protocol 1, both nonuniform attenuation and scatter correction were utilized. Transmission, emission and scatter data were acquired simultaneously with a triple head Picker Prism 3000XP gamma camera. In imaging protocol 2, only nonuniform attenuation correction was applied during the iterative reconstruction. In imaging protocol 3, conventional reconstruction using FBP with low pass postfiltering and uniform attenuation correction ($\mu = 0.11$ cm $^{-1}$) was utilized. The imaging distance was 15.9 cm for protocols 1 and 2 and 13.9 cm for protocol 3. Two 3.6 mm slices were summed and calculation of activity ratios was performed using circular ROIs placed over the spheres and background.

For the sphere with true activity ratio of 9.2, the results for protocols 1, 2 and 3 were 9.3, 8.0

and 6.0, respectively. For the other sphere (true ratio of 4.5), the results were 4.3, 3.7, and 3.0 for protocols 1, 2 and 3. The measured activity ratios of the striatal phantom were 2.4 and 1.6 for protocol 1 and 2.2 and 1.6 for protocol 3. According to these results, transmission imaging based attenuation correction and scatter correction seemed to improve the reliability of ROI based quantification.

3 BRAIN MRI

In MRI, a compromise between signal-to-noise ratio, resolution and imaging time has to be made [47]. Resolution of an MR image can be as good as 1 mm^3 . MRI signal imperfections include noise, intensity nonuniformity and geometrical distortions. The signal-to-noise ratio (SNR) is proportional to the voxel size [48], which also serves as an estimate for spatial resolution in a well-designed system [49]. Sources of intensity nonuniformities in MR images include RF coil nonuniformities, time domain filtering, uncompensated gradient eddy currents, main field nonuniformity and crosstalk between slices [50]. Geometric distortions may be produced by main field inhomogeneity, gradient defects and signal sampling imperfections [49].

3.1 Preprocessing

The purpose of preprocessing is to reduce the impact of factors lowering the quality of images when considering computer assisted analysis. Noise and intensity nonuniformities cause tissue clusters to grow larger, loose tightness and overlap with each other in the feature space. Noise reduction without extensive loss of details can be performed with the anisotropic diffusion method [51]. Besides anisotropic diffusion method, a one pass adaptive Gaussian filter was utilized in Publ. IV prior to the 3D region growing [52].

Different methods for overcoming the problems related to intensity nonuniformity can be found from literature. In phantom methods, a phantom filled with water or oil is imaged and the images are used to estimate the variation in the intensity profile [50, 53]. The gray scales of different slices and different patients have been standardized using a small phantom placed within the RF coil close to the head of a patient [54]. The profile of the inhomogeneities can also be approximated by selecting or segmenting samples from slices and fitting a linear ramp [55], two-dimensional (2D) surface [56, 57] or a 3D function [58] to them. The result from heavy low pass filtering has also been used to estimate inhomogeneities [59]. Homomorphic filtering is a popular approach to implement the separation of the profile found by low pass filtering from the rest of the contents [60, 61, 62]. Also, a proper selection of the samples for the classifier can help to overcome the effects of inhomogeneities [10, 63]. However, according to the comparisons made by Velthuizen et al. [64], these methods can give significantly different correction images, and they suggested that it is not clear whether the RF nonuniformity corrections are in fact yet well understood. In the nonparametric correction method of Sled et al. [65], a model for tissue intensities was derived directly from the data.

Related to Pubs. II and III, methods for reduction of intensity nonuniformity were tested, as only visual evaluation was needed to confirm considerable intensity nonuniformity inside a slice as well as between slices (Figs. 2-4) in these data sets. The sets originated from the Helsinki Stroke Aging Memory (SAM) study [66]. Three spatially matched spin echo images were obtained: proton density weighted (PDw), T2 weighted (T2w) and T1 weighted (T1w). The details of the acquisition parameters have been introduced in Pubs. II and III. Classification of normal and abnormal brain tissue types from these data sets would enable computation of quantitative measures for enhancing diagnosing of dementia using MRI.

Phantom data for estimating the intensity profile were not available from the 2 years' period of imaging the patients of the SAM study. Homomorphic filtering and 2D surface fitting approaches did not produce satisfactory results, as homomorphic filtering lowered the resolution of the image and the result of surface fitting greatly depended on the locations of the fitting points. The surface fitting approach was also considered unsuitable, since in some of the data sets evenly distributed areas of similar tissue (e.g. white matter, WM) did not exist in every slice due to the large infarction regions. Standardization of the gray scales of different slices using a small silicon tube filled with water-MnCl₂ (1 mmol) mixture placed close to the head of a patient was also tested in a few patients and found to be unreliable since the gray value of the tube section varied according to the place in the slice plane indicating that the intensity nonuniformity field was 3D. No correction was finally applied to the images in Pubs. II and III.

3.2 Segmentation

Besides statistical and neural network classification, segmentation methods utilized in brain MRI include thresholding, region growing and histogram based methods [60, 61, 67, 68, 69, 70, 71], edge detection [72] and grouping [73], deformable models [74, 75], contextual classification [76, 77, 78], knowledge-based methods [12, 11] and scale space methods [79]. Most methods are semi-automatic requiring some initial training or manual postprocessing of the results. One approach for segmentation is elastic registration (c.f. Section 4). Many methods are hybrid approaches combining several methods (e.g. [80, 81]).

3.2.1 Statistical and neural network classification

Statistical and neural network classification methods can be divided in two classes depending on whether user interaction is needed in initialization (supervised methods) or not (unsupervised methods, clustering). In supervised methods, the user teaches the system by selecting samples known to belong to a certain tissue class. Thus, the user has control over the clas-

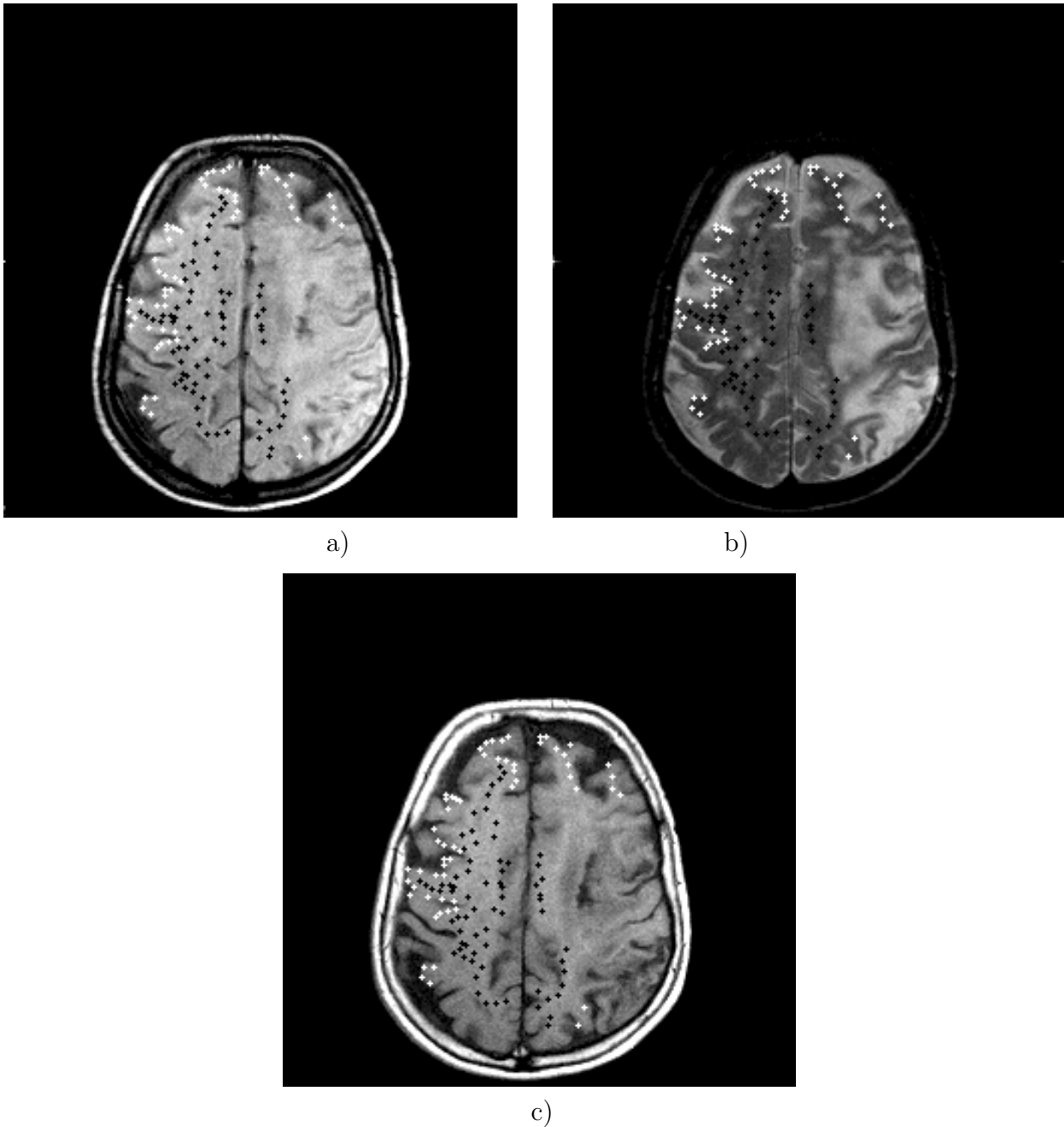


Fig. 2: A a) proton density, b) T2 and c) T1 weighted MRI slice with gray matter (white dots) and white matter (black dots) sample points from a patient with cerebral infarction. Intensity nonuniformity can be seen e.g. as lower intensity values in the left bottom corner of the proton density weighted slice.

sification process. On the other hand, interaction makes the result more reliable on the user and segmentation becomes less automatic. Also, new characteristics of the data unobserved by a human interpreter may be revealed when using unsupervised methods [82].

The most common features used in classification of brain tissues from MR images are the intensity values. If multispectral MRI data are available, a feature vector consisting as many

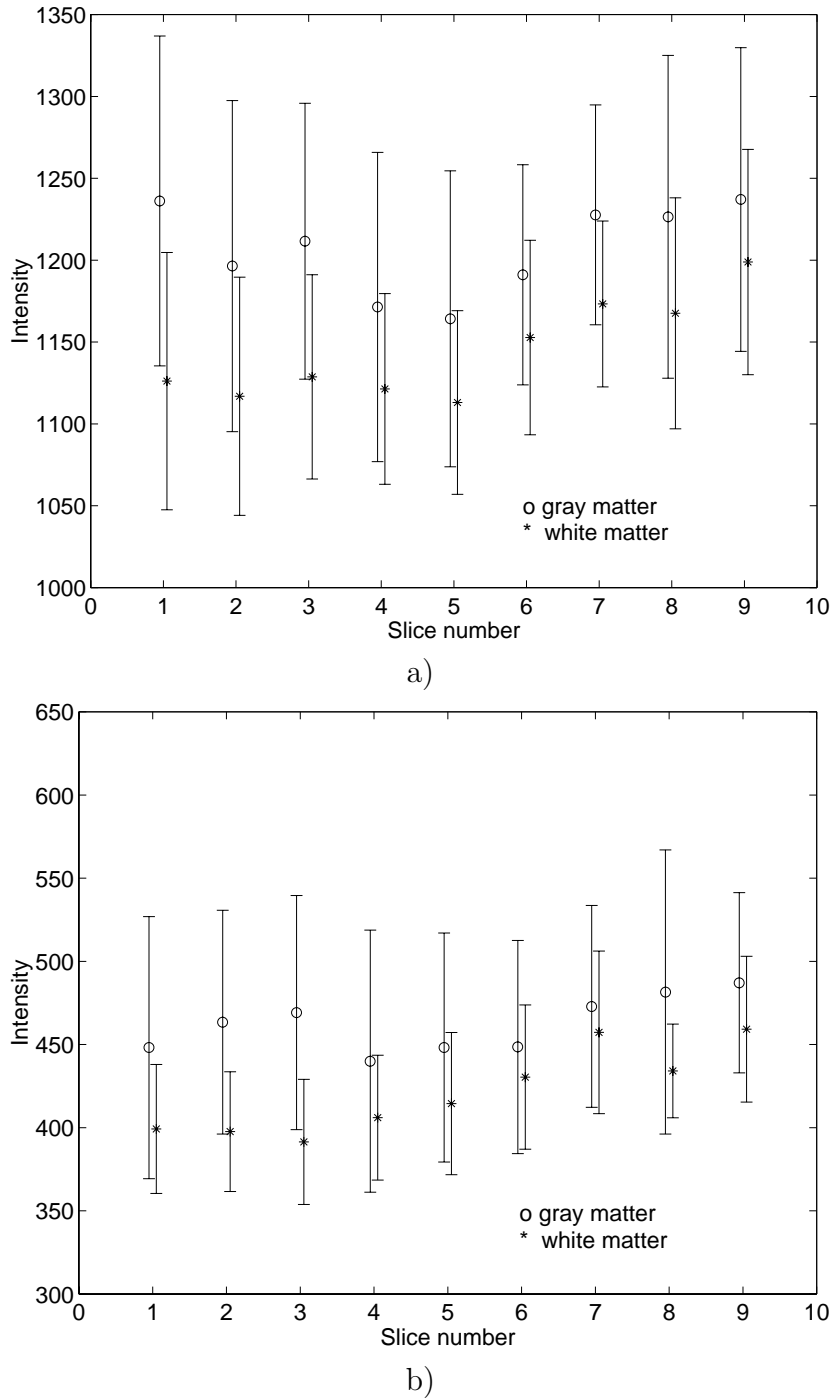


Fig. 3: Mean intensity values and standard deviations of gray and white matter sample points in nine a) proton density and b) T2 weighted slices from the same data set as slices in Fig. 2.

gray values as there are multispectral coregistered images is usually adopted. If other modalities are included in classification, they have to be registered with the MR images as in [10]. Also, linear combinations of the PDw, T2w and T1w images can be utilized [59, 60, 61, 83] although they produce correlated features. Values computed using the neighbourhood of the voxel can be included in the feature vector. This can result in fewer isolated misclassified

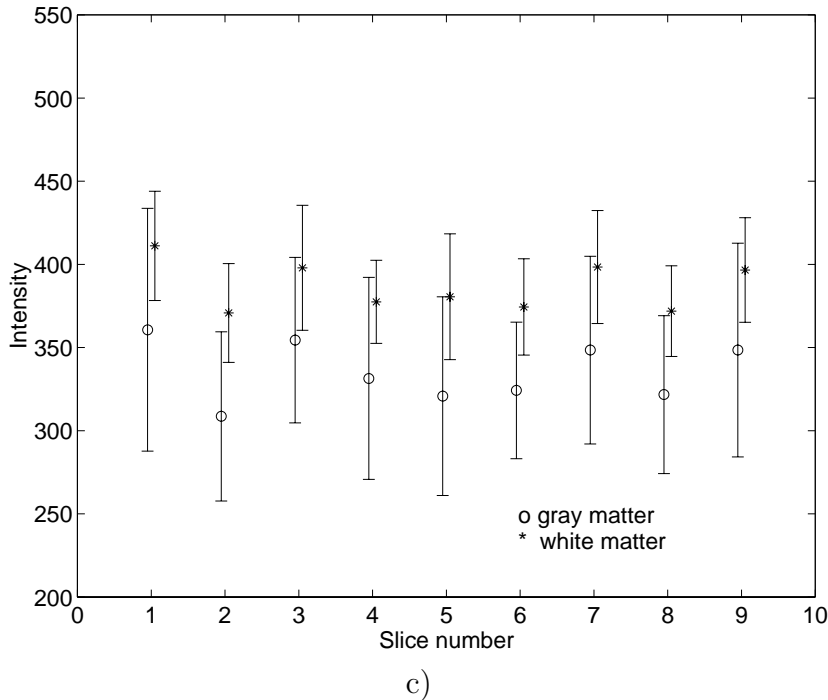


Fig. 4: Same as Fig. 3, but for T1 weighted slices.

voxels (less influence from noise), but on the other hand loss in spatial resolution [10]. The classification of the neighbouring voxels can also be used as one criterion in the classification process resulting in usually iterative contextual methods (e.g. [78, 84]).

Several classification methods have been applied to MR images [85, 86]. Popular supervised statistical classification methods with parameter estimation are the nearest mean and maximum likelihood classifiers [10, 54, 87, 88]. Nonparametric methods include k nearest neighbours (k-NN) classifier [54, 87, 89][Publ. II, Publ. III] and Parzen window techniques [90]. Unsupervised clustering methods can be divided in two classes: algorithms that give crisp labels such as k-means (c-means, minimum distance method) and ISODATA [88, 90, 91], and algorithms producing fuzzy labels such as fuzzy c-means [87, 88, 92, 93]. With fuzzy labelling, a voxel can belong to several classes with different shares. This is one way to deal with voxels affected by the partial volume effect. Neural network classification of the tissues from MR images has often been based on a feedforward network trained with backpropagation [10, 54, 56, 87]. Methods based on self-organizing maps, both unsupervised (SOM) and supervised (LVQ) versions [94], have been utilized [95][Publ. II] as well as the Hopfield [96] and the locally excitatory globally inhibitory oscillator [97] networks. In the adaptive segmentation of Wells et al. [98], a Parzen window technique for classification was utilized iteratively with a Bayesian approach for estimating and correcting intensity nonuniformity field.

In Publ. II, initial experiments were performed to find a reliable classification method for

multispectral data with a visible intensity nonuniformity. Neural network based algorithms were tested since they should be relatively insensitive to selection of the training set [10]. The methods were compared to the widely used k-NN method, which does not make assumptions on the underlying distribution. A SOM [94] based method, a feedforward neural network trained with backpropagation and a 3-NN classifier were utilized. The SOM based method consisted of first training a SOM and detecting the nodes giving ambiguous classification. For these nodes, an additional map was trained using the supervised LVQ algorithm [94] in order to enhance the classification. The pooled form of the 3-NN algorithm [99] consisted of choosing the class with the largest number of samples among the 3 nearest neighbours in the feature space for the voxel to be classified. The feature vector was selected based on the information found from literature. The algorithms were applied mainly to one slice from a multispectral MR image set containing PDw, T2w and T1w images. The accuracy of the classification results was evaluated using a test point set selected by a neuroradiologist. It was found out that the SOM based and the 3-NN methods produced results with almost the same accuracy (about 70-95% for different tissue classes). The backpropagation method produced results with lower accuracy. The stability of the SOM based method was better than the stability of the 3-NN classifier.

In Publ. III, generalization of the methods to interslice and interpatient classification was studied with 10 patient data sets. After initial trials with SOM and LVQ based methods, 5-NN method, and with different feature vectors, the 5-NN method was chosen for classification. The Generalized Mahalanobis Distance [100] was adopted to check whether the quality of the images allowed interslice or interpatient training scheme at all due to intensity nonuniformity in the images. The results indicated that even intraslice training for classification of gray matter (GM) and WM was not necessarily reliable. With interslice training scheme, using a middle slice for training, the mean correct classification rate of all samples given by a neuroradiologist was 85 % for the 10 data sets. Although this percentage was acceptable, the quality of the results was highly variable, as the correct classification rate for one class inside one slice could be as low as 13 %. Thus, the segmentation could not be called operational. To achieve more accurate segmentation, the classification was recommended to be performed slice by slice with user supervision. If better results with less user interaction were required using intensity based classification methods, the images should have had larger intensity differences between the classes. In this work, the required mean intensity difference for GM and WM, to obtain good separability between them, was also computed. The new values produced in fact better separability between GM and all other classes. Besides larger mean intensity differences between classes, smaller variances inside classes would have been produced more reliable classification.

3.2.2 Evaluation of segmentation results

The evaluation of the accuracy of a segmentation result is a complicated task. With patient images the ground truth is not available. With phantom or simulated images the truth is known, but the similarity to patient images may not be close enough due to simpler geometry or difficulties in exact modelling of the NMR signal from different tissues. Usually, the accuracy of a segmentation result is at least assessed visually by a medical expert. Another common procedure is to let a medical expert classify (semi)manually the whole image or some samples from it and to take the classification as a golden standard to which the results are compared (e.g. [10, 50, 55, 56, 76, 88, 101]). Different methods are often compared with each other [10, 54, 87, 102, 103]. The result of classification of tumour images can be based on comparison with the golden standard obtained using contrast agent [54, 87]. In phantom experiments [89, 90, 93, 104] as well as in simulated images [105], the volumes or areas of target tissues are known. Estimates for volumes can also be found from literature [60] although there are individual variances even in normal cases. Individual estimates of the volumes are available from postmortem studies [92, 106]. The accuracy also depends on the modalities available (T1w, T2w and PDw images, CT, etc.) [10, 56]. Besides the accuracy of the result, stability, e.g. to training set in supervised methods, should be checked. The accuracy of classification in Publs. II and III was evaluated by comparing the classification of tests samples to the labelling of them by a neuroradiologist.

4 MULTIMODAL APPROACHES

Selection of a registration method depends on factors such as patient-friendliness, accuracy, speed and interactivity [107]. The application and imaging modalities can also restrict the choice. When registering brain images from different modalities but from the same patient, rigid methods are usually adequate. After a rigid transformation between images I_1 and I_2 has been found, voxels $I_1(\vec{x}_i)$ are transferred to locations $\vec{x}'_j \in I_2$ defined by the following transformation:

$$\vec{x}'_j = \vec{t} + \mathbf{R}\vec{x}_i, \quad (4)$$

where \vec{t} is the translation vector and \mathbf{R} the rotation matrix. Scaling between \vec{x}_i and \vec{x}'_j is not a variable, since voxel dimensions of each image are known.

Computation of the rigid transformation can be based on the use of external artificial markers, attached to the skin or to a stereotactic frame [108, 109, 110, 111][Publ. IV, Publ. VI] or implanted into the skull [112, 113, 114], or on the use of internal anatomy related landmarks [115, 116, 117]. In these cases, a small number (rarely over 15) of corresponding point locations in both images are known, and the transformation is found by an iterative or noniterative fitting of the two point sets. Other approaches are based on choosing features from both images without the knowledge of spatial point-to-point correspondence. Popular features include head or brain surfaces [5, 118, 119, 120, 121, 122], in which case the average point-to-point distance between the corresponding surfaces in the images is iteratively minimized to find the registration transformation. In gray scale correlation methods [7, 123, 124, 125], a measure to be minimized is computed from the intensity values of the images. With specially designed headholders [126, 127, 128, 129], the image sets can be aligned already during the imaging sessions.

In an elastic transformation, a line may be mapped to a curve [130]. Elastic registration is needed for interpatient or patient to atlas registration [131, 132]. Images from human torso may also require elastic registration. In addition, elastic matching can be used for segmentation [133]: after elastic registration of an image to a preclassified object (atlas or another already segmented image), the borders and class labels of different regions can directly be transferred to the volume to be segmented.

In clinical practice, it is important that clear guidelines for imaging exists since there are often special requirements for the images used in registration, depending on the specific application, desired accuracy and imaging modalities. In retrospective registration, the slice thickness should be small enough, and there should be no gaps between the slices, to ensure good resolution in determining the registration transformation and to enable the computation of oblique slices without heavy interpolation. The registration method used may also have

some special requirements. If external markers are utilized, they should not be removed between the imaging sessions to ensure the same placements in different modalities. The requirements must also be adapted to other relevant factors. For example, with modalities using ionizing radiation, patient dose may limit the obtainable resolution.

4.1 Brain SPECT and MRI

Due to the lack of detailed anatomical information in SPECT images, many studies have adopted the use of external markers for registration of SPECT and MR (or CT) images [108, 109, 110][Publ. IV, Publ. VI]. Surface matching methods have also been applied [5, 122, 134, 135]. In surface based approaches, the surface of the brain is usually segmented from both modalities and the surface points are used to find the registration transformation. This type of registration requires accurate segmentation of the brain, which can be a difficult problem with SPECT. In addition, a lesion in the cortex can disturb the registration since it can be differently visible and have a different size in SPECT than in MRI. Gray scale correlation methods have become popular in registration of two SPECT images [7, 136, 137, 138]. This type of registration has also been obtained using principal component analysis for dynamic dopamine receptor studies [139].

In Publ. IV, a registration procedure was implemented to include anatomical information from brain MR images to assist ROI analysis of SPECT images. Registration was based on the use of external skin markers. The markers consisted of plastic tubes filled with a homogenous mixture of coconut butter and $^{99m}\text{TcO}_4^-$. The length of the conical markers was 10 mm and the maximum diameter 4 mm. In patient studies, the number of markers was usually 6. The two marker sets obtained from the images were registered using a noniterative least-squares method [140]. The details of the method have been introduced in Publ. IV. The clinical benefits of registered SPECT and MRI were demonstrated in patients suffering from epilepsy, brain tumour, HSE and cerebral infarction. Different visualization techniques were also demonstrated.

4.2 Registration error

For appropriate clinical use of registration data, an estimate for the spatial errors accumulated to the transformed image during the registration process is needed. If the correct location of a voxel is marked with \vec{x}_j'' and the result from registration with \vec{x}_j' (Eq. 4), the error in location, often referred as a residual, is

$$e_j = |\vec{x}_j'' - \vec{x}_j'|. \quad (5)$$

The root mean squared (RMS) residual of several voxel locations is computed as

$$R = \sqrt{\frac{1}{N} \sum e_j^2}, \quad j = 1, \dots, N, \quad (6)$$

where N is the number of locations included in computation of the RMS error.

In registration of SPECT and MR images using external markers, the locations of the markers in the images are known allowing the determination of the error in these points after the transformation. This error cannot be used as an independent estimate for the accuracy, since the markers have been used for computing the transformation. It still serves as a practical estimate for the success of the registration process, since it indicates the lower bound of the registration error [108][Publ. V]. No measure, except for visual clues, is obtained for the error in ROIs. Several factors affect the error: initial imaging errors in SPECT and MRI, possible movement of patient, skin or the markers during or between imaging sessions, number of markers utilized and their distribution and visibility in the images [Publ. V]. In addition, these factors are filtered through the registration transformation.

Phantom measurements [108, 109, 117, 121, 129, 141][Publ. V] and simulations [112, 116, 117, 141, 142][Publ. V] can be performed to estimate the residuals of known transformed test points. Cadaver studies [112, 143] resemble patient studies but are not suitable for SPECT. Besides visual investigation of patient images, the error can be studied with the help of extra markers attached to the patient [113, 141] or by comparing anatomical details in the case of anatomical images. Different registration methods can also be compared with each other [144, 145, 146]. Correction of geometrical distortions in MRI becomes important in neurosurgery applications with high requirements of registration accuracy [112, 147].

Factors affecting the registration error of brain SPECT and MRI using external markers were studied in Publ. V. Phantom measurements using a dedicated brain phantom and two SPECT and MRI devices were performed. Simulations were also utilized. For the simulations, the error model in external markers was checked using the results from the phantom measurements. The error in the external markers used for registration and in the internal test markers was divided in two parts consisting of a discretizing error due to the inherent discrete size of the voxels and of a locating error due to the finite size of the markers. Errors due to movement of markers or a patient were neglected. Additional errors could be due to artefacts in the images. Details of the phantom measurements and simulations can be found in Publ. V.

In phantom experiments, the RMS error in the test markers inside the phantom was 3-5 mm depending on the imaging equipment and parameters and the number of external markers used in registration. Based on the simulations, about 2 mm in these residuals came from the uncertainty in locating the test markers. The size of the registration error was site

dependent being in its minimum near the centre of mass of the external markers used in registration. When an error comparable to the resolution of the original images (7-10 mm for SPECT, 2 mm for MRI) was included in the test markers, the largest mean RMS residual after registration was smaller than the largest resolution error (9 ± 1 mm). The registration error was not limiting the accuracy of ROI analysis of registered MR and SPECT images, provided that the marker system was properly designed and attached to the patient.

4.3 Transmission imaging for registration

In Publ. VI, SPECT transmission imaging was utilized for registration of ictal and interictal SPECT, MRI and EEG of epileptic patients. The patients were from the epilepsy surgery program of Epilepsy Unit, Hospital of Children and Adolescents, Helsinki University Central Hospital (HUCH). The patients were under video-EEG monitoring when injecting for ictal and interictal SPECT. Both SPECT images were obtained during the same week of long-term monitoring indicating that the electrodes were securely glued during both imaging sessions and not detached in-between. The metallic electrodes were visible in SPECT transmission images (Fig. 5) and utilized as external markers for registration of ictal and interictal SPECT.

Alternative methods for registration of ictal and interictal SPECT include surface fitting [5, 122] and gray scale correlation methods [7, 136]. These methods are practical in the sense that there are no special requirements for the SPECT system. The method developed in this work requires the availability of transmission imaging. The advantages of the method included the determination of the EEG coordinate system in relation to SPECT and MR images without further transformations. As the ictal and interictal SPECT was performed during long-term video-EEG monitoring, the patient always had the electrodes at the scalp at least during the other SPECT study, whether the electrodes were used in registration or not. As the metallic electrodes further attenuate the emission radiation in SPECT, it also seemed important to utilize an accurate attenuation correction method enabled by transmission imaging.

After registration, ictal and interictal SPECT images were scaled to a mean cerebral intensity of 100:

$$I_s(x, y, z) = I_0(x, y, z) * 100/M, \quad (7)$$

where I_s are the scaled and I_0 the original voxel intensities and M the mean cerebral intensity in I_0 [5]. After subtraction of the interictal from the ictal image, the subtraction image was thresholded to include only values greater than 2 standard deviations (SDs) above zero as in [5]. Although the thresholding aimed to minimize the influence of statistical variance in the subtraction image, careful interpretation of the subtraction image was necessary. For

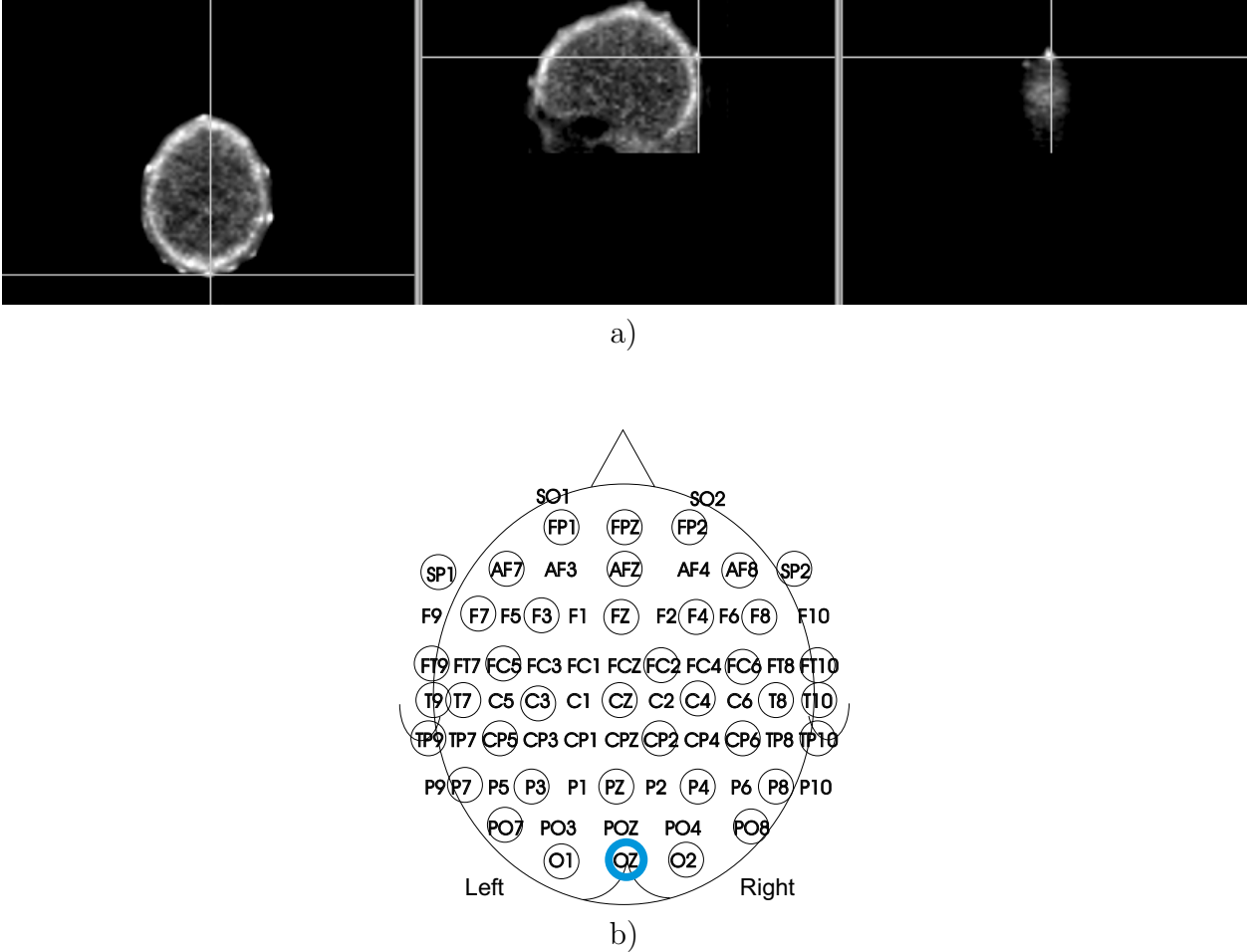


Fig. 5: a) *Transaxial, sagittal and coronal slices from a transmission SPECT image. Electrode OZ has been detected for registration (cross on each slice).* b) *The electrodes used for this patient have been marked with a circle in the electrode map.*

example, besides a threshold value, Zubal et al. [7] included criteria based on the size of the foci and the placement of it (inside gray matter) to decide whether an epileptogenic focus has been detected in the subtraction image.

Registration accuracy in computing the subtraction image should be as good as possible, because even a slight spatial mismatch between the two images to be subtracted can result in a substantial error in the subtracted voxel values [148]. An approach based on external markers has been considered to be an accurate registration method and used as a golden standard for other methods [145, 146], provided that the attachment of the markers is secure. The evaluation of the behaviour of the registration error using external markers and Arun's algorithm [140] was already studied in Publ. V.

The subtraction SPECT image was registered with MRI by fitting the electrode locations to the head surface segmented from MRI. Borgfors' algorithm [149] was utilized for fitting. For error estimation, both ictal and interictal SPECT were separately registered with MRI,

and their electrode locations in the MRI coordinate system were compared. In Publ. VI, utilization of the new registration procedure was demonstrated with five patients. The RMS residual of the registered electrode locations in ictal and interictal SPECT was about 2 mm. When ictal and interictal SPECT were separately registered with MRI, the RMS residual of the electrode locations varied from 3 to 5 mm.

5 CONCLUSIONS

In clinical applications, accuracy and reliability of an image processing method has to be confirmed before using the method. As the ground truth in patient images is not available, tedious phantom experiments and simulations are often needed. Besides them, visual investigation by a medical expert is always utilized. Practical aspects such as special requirements for patient imaging, imaging time and required operator time have also to be considered. Clinical benefits of the method finally state whether extra efforts for image processing should be made. In this section, the main results from sections 2-4 are collected and conclusions on the usability of the methods in clinical environment are made.

The first clinical problem in this thesis was improvement of ROI analysis in SPECT images. Phantom experiments in Publ. I indicated that automatic delineation of ROIs in SPECT images was problematic. Phantom tests in Ref. [40] gave similar results. No single fixed threshold value was found to give a correct volume or a correct activity ratio for two objects. In Publ. I, attenuation was corrected with a method assuming uniform attenuation. Uniform attenuation correction improved the detected activity ratio of objects, but segmentation still remained a problem in Ref. [40]. Correct threshold values depended on filtering and the total activity of the object.

A protocol with transmission imaging based attenuation correction and scatter correction, utilizing an iterative reconstruction algorithm, produced activity ratios of 80 - 100 % of the correct activity ratios in objects representing deep brain structures in Ref. [46]. The conventional protocol with uniform attenuation correction and without scatter correction underestimated the activity ratios (65 - 80 % of the correct ratios). Accurate attenuation and scatter correction increased the reliability of activity measurements using ROIs. Clinical use of transmission imaging and iterative algorithms is still inhibited by longer acquisition and reconstruction times than with conventional protocols.

In Publ. IV, the impact of low resolution and of the lack of detailed anatomical information in SPECT on ROI based analysis was compensated by developing a registration method to include anatomical information from MRI. The clinical benefits of registration were also demonstrated. As SPECT and MRI produced information of very different nature, the complementary information by registration offered help e.g. in analyzing hypoperfusion originally due to cortical atrophy. The utilization of external markers for registration has some practical restrictions. Both SPECT and MRI have to be performed during the same day without detaching the markers. The markers should not disturb the activity distribution of the brain in the SPECT image, while the algorithm for fitting the marker sets requires as widely distributed marker locations as possible to produce accurate results. Transfer of the

images to a separate workstation for registration and the manual localization of the markers from the images cause extra work.

The accuracy of the registration method was studied with phantom experiments and simulations in Publ. V. The registration error inside the phantom was 3-5 mm, of which about 2 mm came from the uncertainty in locating the test markers in the images. The size of the registration error was site dependent being in its minimum near the centre of mass of the external markers used for registration. Even with an error comparable to the resolution of the original images added in the test markers, the largest mean RMS residual after registration was smaller than the resolution of the SPECT images. As a conclusion, the accuracy of the registration procedure did not limit the ROI analysis of registered images, provided that the design and attachment of the marker system were appropriate. Marker movement during or between the imaging sessions was not considered, since it can individually vary from patient to patient. In practice, if a marker is detached for some reason, the movement can be noticed in the images or the marker has dropped off completely. As six markers are usually utilized in patients, two markers can be lost and registration still be obtained. According to the phantom experiments, the accuracy of registration with 4 instead of 6 external markers decreased less than 0.5 mm. Possible patient movement during imaging means lower image quality altogether. The registration procedure was considered to be suitable for clinical use and offered improvement in ROI based analysis of SPECT images.

The second goal was to obtain quantitative information from brain MRI. Opposed to segmentation of SPECT images, volumetric information from MRI is usually considered to be accurate enough, assuming that the resolution is accurately known and geometrical distortions are not significant. The problem lies more in automatic processing of the images, as manual ROI definition from tens or even hundreds of slices is too time-consuming. Automatic methods set quality requirements for the original images. In Publ. II, a SOM based method and a k-NN classifier produced accurate classification results of normal brain tissues as well as tissue types in an infarction region (correct classification rate of 70 - 95 %). The results were obtained for a single slice. Stability of the result was 75 - 82 %.

In Publ. III, interslice training scheme was adopted after a series of tests to check the separability of tissue types in the feature space. The images were suffering from a visible intensity nonuniformity. Using a k-NN method, acceptable (mean correct classification rate of 85 %) but highly variable results were obtained for 10 patient data sets. The tests indicated that intensity differences between tissue types, especially between GM and WM, should be larger or the variances inside classes smaller to obtain reliable segmentation results with an operational intensity based method. To save manual work and to obtain reliable results, the separability of tissue classes should have been checked before imaging a large series of

patients, as the quality requirements for automatic computer based analysis are usually more strict than for visual analysis. In the SAM study, over 400 patients have been imaged using the same equipment and imaging parameters. Extracting quantitative information from these images is possible, but requires more manual work than expected.

The third application in this thesis was localization of epileptogenic foci for epilepsy surgery. Epilepsy surgery candidates usually undergo several imaging examinations for localization of the epileptogenic focus to be removed during surgery. In Publ. VI, a method for registration of ictal and interictal SPECT, MRI and EEG was developed. The methodology was based on SPECT transmission imaging, also allowing as accurate attenuation correction as available to be utilized in reconstruction of the images from patients with metallic electrodes at the scalp. A subtraction SPECT image computed from the ictal and interictal images helped the comparison of the changes in rCBF in these images. The accuracy of registration of ictal and interictal SPECT images was about 2 mm. Careful interpretation of the subtraction image was still needed, as the changes in rCBF depended on the injection time in relation to seizure onset. The accuracy of registration of the subtraction image with MRI was about 3-5 mm. After registration of SPECT images and MRI, the EEG coordinate system was defined in SPECT and MR images without further transformations, providing possibilities for MRI assisted EEG source localization (e.g. [15]).

The inconvenience for the patient from the registration procedure was a longer SPECT imaging time due to transmission imaging. For registration, additional operator time was also required. On the other hand, the extra time required for registration was only a very small part of the total time needed for studying and taking care of a surgery patient, and the registration procedure offered help in spatial localization of the seizure foci.

In this thesis, image processing methods were developed for SPECT and MR images. The methods were validated in clinical environment. The reliability of ROI analysis of SPECT images was enhanced using registration with MRI. Quality requirements for brain MRI data to make segmentation more automatic were evaluated. The registration methodology developed for epilepsy surgery candidates improved the localization of the epileptogenic foci. As a conclusion, improved analysis of SPECT and MR images was obtained with the carefully evaluated methodology presented in this thesis. The registration procedure for brain SPECT and MRI is in clinical use for selected patients in HUCH (currently Health Care Region of Helsinki and Uusimaa), as well as the registration procedure for epilepsy surgery candidates.

6 SUMMARY OF PUBLICATIONS

Publication I: Segmentation methods for volume determination with $^{111}\text{In}/^{99\text{m}}\text{Tc}^m$ SPET (Nucl Med Commun 16:370-377, 1995)

Fixed and adaptive thresholding, region growing and a method combining region growing and edge detection were tested on phantom and patient images obtained with $^{99\text{m}}\text{Tc}$ and ^{111}In SPECT (SPET). None of the tested methods produced accurate or stable results. Fixed thresholding and region growing may be adaptable for segmenting clinical images, if the parameters are optimized using phantom experiments. Preferably, the object boundaries have to be included from anatomical modalities using registration.

Errata: In page 371 in section Results, the sentence “Using RGE, the gradient chosen was 0.5.” should be “Using RGE, the weight ϕ of the gradient was chosen to be 0.5.”.

Publication II: Stability study of some neural networks applied to tissue characterization of brain magnetic resonance images (Proceedings of the IAPR 13th International Conference on Pattern Recognition, Vol. IV, 472-477, 1996)

A SOM based method was compared with a feedforward neural network trained with back-propagation and a k-NN classifier for tissue classification from multispectral MR images. The algorithms were tested on spatially matched PDw, T2w and T1w slices from a patient suffering from cerebral infarction. The most accurate results were achieved with the SOM based method and with the k-NN classifier. The SOM based method was the most stable method.

Publication III: Experiences on data quality in automatic tissue classification (Report TKK-F-A794, Helsinki University of Technology, 1999)

Tests for evaluating the separability of tissue classes in multispectral MR images, and on the other hand class distances required to obtain reliable classification, were presented in this paper. Intraslice, interslice and interpatient training schemes for 5-nn classification were considered. Interslice training was utilized in classification of images from 10 patients with ischemic stroke giving results of satisfactory but highly variable quality, indicating that operational intensity based classification was not possible. Based on the experience with these data sets, similar tests were recommended before imaging a large patient series in order to avoid extra manual work and to obtain reliable classification results.

Publication IV: Registration and display of brain SPECT and MRI using external markers (Neuroradiology 38:108-114, 1996)

A registration system based on external markers and on a noniterative least-squares method for brain SPECT and MRI was developed. The clinical benefits of registration were demonstrated with images from patients suffering from epilepsy, encephalitis, brain tumour and

cerebral infarction. Different visualization techniques for registered information were introduced.

Errata: Theoretically three markers are adequate for the registration, if they are not colinear.

Publication V: Accuracy of a registration procedure for brain SPET and MRI: phantom and simulation studies (Nucl Med Commun 18:517-526, 1997)

The accuracy of the registration protocol introduced in Publ. IV was evaluated using phantom measurements and simulations. The error model for the simulations was verified by the results from the phantom experiments. It was concluded that the registration accuracy was not the limiting factor in ROI analysis of the registered images provided that the external marker system was properly designed and attached. The major error source was the modest spatial resolution of SPECT (SPET).

Errata: In Table 1, under Phantom Experiment A, MRI, instead of the latter Study A1 there should read Study A2.

Publication VI: Transmission imaging for registration of ictal and interictal single-photon emission tomography, magnetic resonance imaging and electroencephalography (Eur J Nucl Med 27:202-205, 2000)

A method for registration of ictal and interictal SPECT, MRI and EEG was developed. For SPECT studies, ^{99m}Tc -ECD was injected intravenously while the patient was monitored on video-EEG to document ictal or interictal state. Imaging was performed using a triple-head gamma camera equipped with a transmission imaging device. The gold plated silver electrodes at the patient's scalp, visible in the transmission images, were utilized as markers for registration of the ictal and interictal SPECT images. The interictal SPECT image was subtracted from the ictal image after scaling. For registration of MR and subtraction SPECT images, the external marker set of the ictal SPECT study was fitted to the surface of the head from MRI. The estimated RMS error of registration in the final result combining locations of the electrodes, subtraction SPECT and MR images was 3-5 mm.

References

- [1] Webb S. *The Physics of Medical Imaging*. IOP Publishing Ltd, 1988.
- [2] Duncan JS. Imaging and epilepsy. *Brain* 1997; **120**:339–377.
- [3] Launes J, Nikkinen P, Lindroth L, *et al.* Brain perfusion defect size in SPECT predicts outcome in cerebral infarction. *Nucl Med Commun* 1989; **10**:891–900.
- [4] Launes J, Nikkinen P, Lindroth L, *et al.* Diagnosis in acute herpes simplex encephalitis by brain perfusion SPECT. *The Lancet* 1988; **i**:1188–1191.
- [5] O’Brien TJ, O’Connor MK, Mullan BP, *et al.* Subtraction ictal SPECT co-registered to MRI in partial epilepsy: Description and technical validation of the method with phantom and patient studies. *Nucl Med Commun* 1998; **19**:31–45.
- [6] Nikkinen P. *Single Photon Emission Tomography in Neurological Studies: Instrumentation and Clinical Applications*, PhD Thesis, Helsinki University. 1999.
- [7] Zubal IG, Spanaki MV, MacMullan J, *et al.* Influence of technetium-99m-hexamethylpropylene amine oxime injection time on single-photon emission tomography perfusion changes in epilepsy. *Eur J Nucl Med* 1999; **26**:12–17.
- [8] Pykett IL, Newhouse JH, Buonanno FS, *et al.* Principles of nuclear magnetic resonance imaging. *Radiology* 1982; **143**:157–168.
- [9] Twieg DB. The k-trajectory formulation of the NMR imaging process with applications in analysis and synthesis of imaging methods. *Med Phys* 1983; **10**:610–621.
- [10] Özkan M, Dawant BM, Maciunas RJ. Neural-network-based segmentation of multi-modal medical images: A comparative and prospective study. *IEEE Trans Med Imaging* 1993; **12**:534–544.
- [11] Clarke LP, Velthuizen RP, Clark M, *et al.* MRI measurement of brain tumor response: Comparison of visual metric and automatic segmentation. *Magn Reson Imaging* 1998; **16**:271–279.
- [12] Clark MC, Hall LO, Goldgof DB, *et al.* Automatic tumor segmentation using knowledge-based techniques. *IEEE Trans Med Imaging* 1998; **17**:187–201.
- [13] Kikinis R, Guttmann CRG, Metcalf D, *et al.* Quantitative follow-up of patients with multiple sclerosis using MRI: Technical aspects. *J Magn Reson Imaging* 1999; **9**:519–530.
- [14] Lawrie SM, Abukmeil SS. Brain abnormality in schizophrenia. A systematic and quantitative review of volumetric magnetic resonance imaging studies. *Br J Psychiatry* 1998; **172**:110–120.
- [15] Huppertz HJ, Otte M, Grimm C, *et al.* Estimation of the accuracy of a surface matching technique for registration of EEG and MRI data. *Electroenceph Clin Neurophysiol* 1998; **106**:409–415.

- [16] Larsson SA. Gamma Camera Emission Tomography. *Acta Radiologica Supplementum* 363, 1980.
- [17] Knoll GF. Single-photon emission computed tomography. In: *Proceedings of the IEEE, Vol. 71, No. 3*, 1983.
- [18] Kak AC, Slaney M. Principles of Computerized Tomographic Imaging, Ch. 3. New York: IEEE Press, 1988.
- [19] Chornoboy ES, Chen CJ, Miller MI, *et al.* An evaluation of maximum likelihood reconstruction for SPECT. *IEEE Trans Med Imaging* 1990; **9**:99–110.
- [20] Kauppinen T. Improvement of SPECT Imaging Using Iterative Reconstruction, PhD Thesis, Kuopio University. 1999.
- [21] Blockland KAK, Reiber HHC, Pauwels EKJ. Quantitative analysis in single photon emission tomography (SPET). *Eur J Nucl Med* 1992; **19**:47–61.
- [22] Müller SP, Kijewski MF, Moore SC, *et al.* Maximum-likelihood estimation: A mathematical model for quantitation in nuclear medicine. *J Nucl Med* 1990; **31**:1693–1701.
- [23] Madsen MT, Chang W, Hichwa RD. Spatial resolution and count density requirements in brain SPECT imaging. *Phys Med Biol* 1992; **37**:1625–1636.
- [24] Moore SC, Kouris K, Cullum I. Collimator design for single photon emission tomography. *Eur J Nucl Med* 1992; **19**:138–150.
- [25] Rosenthal MS, Cullom J, Hawkins W, *et al.* Quantitative SPECT imaging: A review and recommendations by the focus committee of the Society of Nuclear Medicine Computer and Instrumentation Council. *J Nucl Med* 1995; **36**:1489–1513.
- [26] Bieszka JA, Hawman EG. Evaluation of SPECT angular sampling effects: Continuous versus step-and-shoot acquisition. *J Nucl Med* 1987; **28**:1308–1314.
- [27] Smith MF, Floyd CE, Jaszczak RJ, *et al.* Reconstruction of SPECT images using generalized matrix inverses. *IEEE Trans Med Imaging* 1992; **11**:165–184.
- [28] Bailey DL. Transmission scanning in emission tomography. *Eur J Nucl Med* 1998; **25**:774–787.
- [29] Msaki P, Axelsson B, Larsson SA. Some physical factors influencing the accuracy of convolution scatter correction in SPECT. *Phys Med Biol* 1989; **34**:283–298.
- [30] Buvat I, Benali H, Todd-Pokropek A, *et al.* Scatter correction in scintigraphy: The state of art. *Eur J Nucl Med* 1994; **21**:675–694.
- [31] Mortelmans L, Nuyts J, Pamel GV, *et al.* A new thresholding method for volume determination by SPECT. *Eur J Nucl Med* 1986; **12**:284–290.
- [32] Long DT, King MA, Sheehan J. Comparative evaluation of image segmentation methods for volume quantitation in SPECT. *Med Phys* 1992; **19**:483–489.
- [33] Groshar D, Frankel A, Iosilevsky G, *et al.* Quantitation of renal uptake of technetium-99m DMSA using SPECT. *J Nucl Med* 1989; **30**:246–250.

- [34] Savolainen S. SPECT versus planar scintigraphy for quantification of splenic sequestration of ^{111}In -labelled platelets. *Nucl Med Commun* 1992; **13**:757–763.
- [35] Alaamer AS, Fleming JS, Perring S. Evaluation of the factors affecting the accuracy and precision of a technique for quantitation of volume and activity in SPECT. *Nucl Med Commun* 1994; **15**:758–771.
- [36] Fleming JS, Alaamer AS. A rule based method for context sensitive threshold segmentation in SPECT using simulation. *Phys Med Biol* 1998; **43**:2309–2323.
- [37] Kircos LT, Carey, Jr. JE, Keyes, Jr. JW. Quantitative organ visualization using SPECT. *J Nucl Med* 1987; **28**:334–341.
- [38] Acton PD, Pilowsky LS, Kung HF, *et al.* Automatic segmentation of dynamic neuroreceptor single-photon emission tomography images using fuzzy clustering. *Eur J Nucl Med* 1999; **26**:581–590.
- [39] Fleming JS, Kemp PM, Bolt L. A technique for manual definition of an irregular volume of interest in single photon emission computed tomography. *Phys Med Biol* 1999; **44**:N15–N20.
- [40] Sipilä O, Kortensniemi M, Nikkinen P, *et al.* Optimizing a protocol for Tc-99m-DMSA SPET studies. *Eur J Nucl Med* 1997; **24**:1055.
- [41] Picker International, Inc., Nuclear Medicine Division, Cleveland, Ohio. Picker Nuclear Medical Imaging Systems, Odyssey VP, Operator's Guide, Vol. 1, 1995.
- [42] Yang J. A Single Isotope Method for Simultaneous Emission and Transmission Scatter Correction in SPECT, PhD Thesis, Kuopio University. 1999.
- [43] Tung CH, Gullberg GT, Zeng GL, *et al.* Non-Uniform attenuation correction using simultaneous transmission and emission converging tomography. *IEEE Trans Nucl Sci* 1992; **39**:1134–1143.
- [44] Picker International, Inc., Nuclear Medicine Division, Cleveland, Ohio. STEP for Prism 3000XP, Operator's Guide, 1995.
- [45] Maniawski P, Miller S. Combined attenuation and scatter correction with transmission emission SPECT system (STEP) - practical implementation and phantom evaluation. *Eur J Nucl Med* 1996; **23**:1123.
- [46] Nikkinen P, Sipilä O, Savolainen S. Comparison of transmission imaging based and conventional acquisition modes in brain basal ganglia phantom studies. *Eur J Nucl Med* 1999; **26**:1039.
- [47] Constable RT, Henkelman RM. Contrast, resolution and detectability in MR imaging. *J Comput Assist Tomogr* 1991; **15**:297–303.
- [48] Edelstein WA, Glover GH, Hardy CJ, *et al.* The intrinsic signal-to-noise ratio in NMR imaging. *Magn Reson Med* 1986; **3**:604–618.

- [49] Lerski RA, de Certaines JD. II. Performance assessment and quality control in MRI by eurospin test objects and protocols. *Magn Reson Imaging* 1993; **11**:817–833.
- [50] Simmons A, Arridge SR, Barker GJ, *et al.* Improvements to the quality of MRI cluster analysis. *Magn Reson Imaging* 1994; **12**:1191–1204.
- [51] Gerig G, Kübler O, Kikinis R, *et al.* Nonlinear anisotropic filtering of MRI data. *IEEE Trans Med Imaging* 1992; **11**:221–232.
- [52] Sipilä O, Vehkomäki T, Salli E, *et al.* General tools for segmentation. In: *Proceedings of the IEEE EMBS Satellite Symposium on 3D Advanced Image Processing in Medicine*. 1992; 197–199.
- [53] Rusinek H, de Leon MJ, George AE, *et al.* Alzheimer disease: Measuring loss of cerebral gray matter with MR imaging. *Neuroradiology* 1991; **178**:109–114.
- [54] Clarke LP, Velthuizen RP, Phuphanich S, *et al.* MRI: Stability of three supervised segmentation techniques. *Magn Reson Imaging* 1993; **11**:95–106.
- [55] Vannier MW, Pilgram TK, Speidel CM, *et al.* Validation of magnetic resonance imaging MRI multispectral tissue classification. *Comput Med Imag Grap* 1991; **15**:217–223.
- [56] Zijdenbos AP, Dawant BM, Margolin RA, *et al.* Morphometric analysis of white matter lesions in MR images: Method and validation. *IEEE Trans Med Imaging* 1994; **13**:716–724.
- [57] Dawant BM, Zijdenbos AP, Margolin RA. Correction of intensity variations in MR images for computer-aided tissue classification. *IEEE Trans Med Imaging* 1993; **12**:770–781.
- [58] Meyer CR, Bland PH, Pipe J. Retrospective correction of intensity inhomogeneities in MRI. *IEEE Trans Med Imaging* 1995; **14**:36–41.
- [59] Jernigan TL, Press GA, Hesselink JR. Methods for measuring brain morphologic features on magnetic resonance images. *Arch Neurol* 1990; **47**:27–32.
- [60] Lim KO, Pfefferbaum A. Segmentation of MR brain images into cerebrospinal fluid spaces, white and gray matter. *J Comput Assist Tomogr* 1989; **13**:588–593.
- [61] Harris GJ, Bart PE, Peng LW, *et al.* MR volume segmentation of gray matter and white matter using manual thresholding: Dependence on image brightness. *AJNR* 1994; **15**:225–230.
- [62] Brinkmann BH, Manduca A, Robb RA. Optimized homomorphic unsharp masking for MR grayscale inhomogeneity correction. *IEEE Trans Med Imaging* 1998; **17**:161–171.
- [63] Cline HE, Lorensen WE, Kikinis R, *et al.* Three-dimensional segmentation of MR images of the head using probability and connectivity. *J Comput Assist Tomogr* 1990; **14**:1037–1045.
- [64] Velthuizen RP, Heine JJ, Cantor AB, *et al.* Review and evaluation of MRI uniformity corrections for brain tumor response measurements. *Med Phys* 1998; **25**:1655–1666.

- [65] Sled JG, Zijdenbos AP, Evans AC. A nonparametric method for automatic correction of intensity nonuniformity in MRI data. *IEEE Trans Med Imaging* 1998; **17**:87–97.
- [66] Pohjasvaara T, Erkinjuntti T, Vataja R, *et al.* Dementia three months after stroke: Baseline frequency and effect of different definitions of dementia in the Helsinki Stroke Aging Memory Study (SAM) cohort. *Stroke* 1997; **28**:785–792.
- [67] Schroeter P, Vesin JM, R. Meuli TL. Robust parameter estimation of intensity distributions for brain magnetic resonance images. *IEEE Trans Med Imaging* 1998; **17**:172–186.
- [68] Brummer ME, Mersereau RM, Eisner RL, *et al.* Automatic detection of brain contours in MRI data sets. *IEEE Trans Med Imaging* 1993; **12**:153–166.
- [69] Pannizzo F, Stallmeyer MJB, Friedman J, *et al.* Quantitative MRI studies for assessment of multiple sclerosis. *Magn Reson Med* 1992; **24**:90–99.
- [70] Lemieux L, Hagemann G, Krakow K, *et al.* Fast, accurate, and reproducible automatic segmentation of the brain in T₁-weighted volume MRI data. *Magn Reson Med* 1999; **42**:127–135.
- [71] Woermann FG, Sisodiya SM, Free SL, *et al.* Quantitative MRI in patients with idiopathic generalized epilepsy. *Brain* 1998; **121**:1661–1667.
- [72] Bomans M, Höhne KH, Tiede U, *et al.* 3-D segmentation of MR images of the head for 3-D display. *IEEE Trans Med Imaging* 1990; **9**:177–183.
- [73] Vehkomäki T. Image Segmentation by Contour Grouping: Knowledge Based Search in Attributed Proximity Graph, PhD Thesis. Acta Polytechnica Scandinavica Ma 76, 1995.
- [74] McInerney T, Terzopoulos D. Deformable models in medical image analysis: A survey. *Medical Image Analysis* 1996; **1**:91–108.
- [75] Lötjönen J, Reissman PR, Magnin IE, *et al.* Model extraction from magnetic resonance volume data using the deformable pyramid. *Med Image Anal* 1999; **3**:387–406.
- [76] Taxt T, Lundervold A. Multispectral analysis of the brain using magnetic resonance imaging. *IEEE Trans Med Imaging* 1994; **13**:470–481.
- [77] Liang Z, MacFall JR, Harrington DP. Parameter estimation and tissue segmentation from multispectral MR images. *IEEE Trans Med Imaging* 1994; **13**:441–449.
- [78] Held K, Kops ER, Krause BJ, *et al.* Markov random field segmentation of brain MR images. *IEEE Trans Med Imaging* 1997; **16**:878–886.
- [79] Simmons A, Arridge SR, Tofts PS, *et al.* Application of the extremum stack to neurological MRI. *IEEE Trans Med Imaging* 1998; **17**:371–382.
- [80] Atkins MS, Mackiewich BT. Fully automatic segmentation of the brain in MRI. *IEEE Trans Med Imaging* 1998; **17**:98–107.

- [81] Heinonen T, Dastidar P, Kauppinen P, *et al.* Semi-automatic tool for segmentation and volumetric analysis of medical images. *Med Biol Eng Comput* 1998; **36**:291–296.
- [82] Gerig G, Martin J, Kikinis R, *et al.* Segmentation of dual-echo MR head data. In: Lemke HU, Rhodes ML, Jaffe CC, *et al.*, eds., *Computer Assisted Radiology, CAR'91*. Berlin Heidelberg: Springer-Verlag, 1991; 606–611.
- [83] Raya SP. Low-level segmentation of 3-D magnetic resonance brain images - a rule-based system. *IEEE Trans Med Imaging* 1990; **9**:327–337.
- [84] Johnston B, Atkins MS, Mackiewich B, *et al.* Segmentation of multiple sclerosis lesions in intensity corrected multispectral MRI. *IEEE Trans Med Imaging* 1996; **15**:154–169.
- [85] Bezdek JC, Hall LO, Clarke LP. Review of MR image segmentation techniques using pattern recognition. *Med Phys* 1993; **20**:1033–1048.
- [86] Clarke LP, Velthuizen RP, Camacho MA, *et al.* MRI segmentation: Methods and applications. *Magn Reson Imaging* 1995; **13**:343–368.
- [87] Clarke LP, Velthuizen RP, Hall LO, *et al.* Comparison of supervised pattern recognition techniques and unsupervised methods for MRI segmentation. In: *SPIE Vol. 1652 Medical Imaging VI: Image Processing*. 1992; 668–677.
- [88] DeLaPaz RL, Herskovits E, Gesu VD, *et al.* Cluster analysis of medical magnetic resonance images MRI data: Diagnostic application and evaluation. In: *SPIE Vol. 1259 Extracting Meaning from Complex Data: Processing, Display, Interaction*. 1990; 176–181.
- [89] Jackson EF, Narayana PA, Wolinsky JS, *et al.* Accuracy and reproducibility in volumetric analysis of multiple sclerosis lesions. *J Comput Assist Tomogr* 1993; **17**:200–205.
- [90] Gerig G, Martin J, Kikinis R, *et al.* Unsupervised tissue type segmentation of 3D dual-echo MR head data. *Image Vision Comput* 1992; **10**:349–360.
- [91] Nagesh V, Welch KMA, Windham JP, *et al.* Time course of ADCw changes in ischemic stroke: Beyond the human eye! *Stroke* 1998; **29**:1778–1782.
- [92] Phillips WE, Velthuizen RP, Phuphanich S, *et al.* Application of fuzzy c-means segmentation technique for tissue differentiation in MR images of a hemorrhagic glioblastoma multiforme. *Magn Reson Imaging* 1995; **13**:277–290.
- [93] Brandt ME, Bohan TP, Kramer LA, *et al.* Estimation of CSF, white and gray matter volumes in hydrocephalic children using fuzzy clustering of MR images. *Comput Med Imag Grap* 1994; **18**:25–34.
- [94] Kohonen T. *Self-Organizing Maps*. Berlin Heidelberg: Springer-Verlag, 1995.
- [95] Reddick WE, Glass JO, Cook EN, *et al.* Automated segmentation and classification of multispectral magnetic resonance images of brain using artificial neural networks. *IEEE Trans Med Imaging* 1997; **16**:911–918.

- [96] Amartur SC, Piraino D, Takefuji Y. Optimization neural networks for the segmentation of magnetic resonance images. *IEEE Trans Med Imaging* 1992; **11**:215–220.
- [97] Shareef N, Wang DL, Yagel R. Segmentation of medical images using LEGION. *IEEE Trans Med Imaging* 1999; **18**:74–91.
- [98] Wells WM, III, Grimson WEL, Kikinis R, *et al.* Adaptive segmentation of MRI data. *IEEE Trans Med Imaging* 1996; **15**:429–442.
- [99] Therrien CW. Decision Estimation and Classification: An Introduction to Pattern Recognition and Related Topics, Ch. 8. New York: John Wiley & Sons, Inc., 1989.
- [100] Taxt T, Olafsdottir JB, Daehlen M. Recognition of handwritten symbols. *Pattern Recognition* 1990; **23**:1155–1166.
- [101] Vannier MW, Speidel CM, Rickman DL. Magnetic resonance imaging multispectral tissue classification. *NIPS* 1988; **3**:148–154.
- [102] Hall LO, Bensaid AM, Clarke LP, *et al.* A comparison of neural network and fuzzy clustering techniques in segmenting magnetic resonance images of the brain. *IEEE Trans Neural Networks* 1992; **5**:672–682.
- [103] Vaidyanathan M, Clarke LP, Heidtman C, *et al.* Normal brain volume measurements using multispectral MRI segmentation. *Magn Reson Imaging* 1997; **15**:87–97.
- [104] Kohn MI, Tanna NK, Herman GT, *et al.* Analysis of brain and cerebrospinal fluid volumes with MR imaging; Part I. methods, reliability, and validation. *Radiology* 1991; **178**:115–122.
- [105] Choi HS, Haynor DR, Kim Y. Multivariate tissue classification of MRI images for 3-D volume reconstruction - a statistical approach. In: *SPIE Vol. 1092 Medical Imaging III: Image Processing*. 1989; 183–193.
- [106] Bartlett TQ, Vannier MW, McKeel, Jr. DW, *et al.* Interactive segmentation of cerebral gray matter, white matter, and CSF: Photographic and MR images. *Comput Med Imag Grap* 1994; **18**:449–460.
- [107] van den Elsen PA, Pol EJD, Viergever MA. Medical image matching - a review with classification. *IEEE Eng Med Biol* 1993; **12**:26–39.
- [108] Malison RT, Miller EG, Greene R, *et al.* Computer-assisted coregistration of multislice SPECT and MR brain images by fixed external fiducials. *J Comput Assist Tomogr* 1993; **17**:952–960.
- [109] Erickson BJ, Jack CR. Correlation of single photon emission CT and MR image data using fiduciary markers. *AJNR* 1993; **14**:713–720.
- [110] van den Elsen PA, Viergever MA. Marker-guided multimodality matching of the brain. *Eur Radiol* 1994; **4**:45–51.
- [111] Pohjonen H. Image Fusion in Open-Architecture Quality-Oriented Nuclear Medicine and Radiology Departments, PhD Thesis, Helsinki University of Technology. 1997.

- [112] Maurer CR, Fitzpatrick JM, Wang MY, *et al.* Registration of head volume images using implantable fiducial markers. *IEEE Trans Med Imaging* 1997; **16**:447–462.
- [113] Maurer CR, Aboutanos GB, Dawant BM, *et al.* Effect of geometrical distortion correction in MR on image registration accuracy. *J Comput Assist Tomogr* 1996; **20**:666–679.
- [114] Wang MY, Maurer CR, Fitzpatrick JM, *et al.* An automatic technique for finding and localizing externally attached markers in CT and MR volume images of the head. *IEEE Trans Biomed Eng* 1996; **43**:627–637.
- [115] Hill DLG, Hawkes DJ, Crossman JE, *et al.* Registration of MR and CT images for skull base surgery using point-like anatomical features. *Br J Radiol* 1991; **64**:1030–1035.
- [116] Neelin P, Crossman J, Hawkes DJ, *et al.* Validation of an MR/PET landmark registration method using 3-D simulated PET images and point simulations. In: Roux C, Herman GT, Collorec R, eds., *Proceedings of the IEEE EMBS Satellite Symposium on 3D Advanced Image Processing in Medicine*. 1992; 73–77.
- [117] Hill DLG, Hawkes DJ, Gleeson MJ, *et al.* Accurate frameless registration of MR and CT images of the head: Applications in surgery and radiotherapy planning. *Radiology* 1994; **191**:447–454.
- [118] Pelizzari CA, Chen GTY, Spelbring DR, *et al.* Accurate three-dimensional registration of CT, PET, and/or MR images of the brain. *J Comput Assist Tomogr* 1989; **13**:20–26.
- [119] Collignon A, Vandermeulen D, Suetens P, *et al.* Registration of 3D multi-modality medical images using surfaces and point landmarks. *Patt Recogn Lett* 1994; **15**:461–467.
- [120] Mazziotta JC, Pelizzari CC, Chen GT, *et al.* Region of interest issues: The relationship between structure and function in the brain. *J Cereb Blood Flow Metab* 199; **11**:A51–A56.
- [121] Turkington TG, Hoffman JM, Jaszczak RJ, *et al.* Accuracy of surface fit registration for PET and MR brain images using full and incomplete brain surfaces. *J Comput Assist Tomogr* 1995; **19**:117–124.
- [122] Zubal IG, Spencer SS, Imam K, *et al.* Difference images calculated from ictal and interictal technetium-99m-HMPAO SPECT scans of epilepsy. *J Nucl Med* 1995; **36**:684–689.
- [123] Woods RP, Mazziotta JC, Cherry SR. MRI-PET registration with automated algorithm. *J Comput Assist Tomogr* 1993; **17**:536–546.
- [124] Hajnal JV, Saeed N, Soar EJ, *et al.* A registration and interpolation procedure for subvoxel matching of serially acquired MR images. *J Comput Assist Tomogr* 1995; **19**:289–296.

- [125] Nikou C, Heitz F, Armspach JP, *et al.* Registration of MR/MR and MR/SPECT brain images by fast stochastic optimization of robust voxel similarity measures. *Neuroimage* 1998; **8**:30–43.
- [126] Bergström M, Boëthius J, Eriksson L, *et al.* Head fixation device for reproducible position alignment in transmission CT and positron emission tomography. *J Comput Assist Tomogr* 1981; **5**:136–141.
- [127] Miura S, Kanno I, Iida H, *et al.* Anatomical adjustments in brain positron emission tomography using CT images. *J Comput Assist Tomogr* 1998; **12**:363–367.
- [128] Bettinardi V, Scardaoni R, Gilardi MC, *et al.* Head holder for PET, CT, and MR studies. *J Comput Assist Tomogr* 1991; **15**:886–892.
- [129] Metzger CC, Bryan RN, Holcomb HH, *et al.* Anatomical localization for PET using MR imaging. *J Comput Assist Tomogr* 1990; **14**:418–426.
- [130] Maintz JBA, Viergever MA. A survey of medical image registration. *Med Image Anal* 1998; **2**:1–36.
- [131] Gee JC, Reivich M, Bajcsy R. Elastically deforming 3D atlas to match anatomical brain images. *J Comput Assist Tomogr* 1993; **17**:225–236.
- [132] Iosifescu DV, Shenton ME, Warfield SK, *et al.* An automated registration algorithm for measuring MRI subcortical brain structures. *Neuroimage* 1997; **6**:13–25.
- [133] Collins DL, Holmes CJ, Peters TM, *et al.* Automatic 3-D model-based neuroanatomical segmentation. *Human Brain Mapping* 1995; **3**:190–208.
- [134] Holman BL, Jonson REZKA, Carvalho PA, *et al.* Computer-assisted superimposition of magnetic resonance and high-resolution technetium-99m-HMPAO and thallium-201 SPECT images of the brain. *J Nucl Med* 1991; **32**:1478–1484.
- [135] van Herk M, Kooy HM. Automatic three-dimensional correlation of CT-CT, CT-MRI, and CT-SPECT using chamfer matching. *Med Phys* 1992; **21**:1163–1176.
- [136] Brinkmann BH, O’Brien TJ, Aharon S, *et al.* Quantitative and clinical analysis of SPECT image registration for epilepsy studies. *J Nucl Med* 1999; **40**:1098–1105.
- [137] Imran MB, Kawashima R, Sato K, *et al.* Mean regional cerebral blood flow images of normal subjects using technetium-99m-HMPAO by automated image registration. *J Nucl Med* 1997; **39**:203–207.
- [138] Imran MB, Kawashima R, Awata S, *et al.* Parametric mapping of cerebral blood flow defects in Alzheimer’s disease: A SPECT study using HMPAO and image standardization technique. *J Nucl Med* 1999; **40**:244–249.
- [139] Acton PD, Pilowsky LS, Suckling J, *et al.* Registration of dynamic dopamine D₂ receptor images using principal component analysis. *Eur J Nucl Med* 1997; **24**:1405–1412.

- [140] Arun KS, Huang TS, Blostein SD. Least-squares fitting of two 3-D point sets. *IEEE Trans PAMI* 1987; **9**:698–700.
- [141] Maurer CM, Fitzpatrick JM, Galloway RL, *et al.* The accuracy of image-guided neurosurgery using implantable fiducial markers. In: Lemke HU, Inamura K, Jaffe CC, *et al.*, eds., *Computer Assisted Radiology, CAR'95*. Berlin Heidelberg: Springer-Verlag, 1995; 1197–1202.
- [142] Evans AC, Marret S, Torrescorzo J, *et al.* MRI-PET correlation in three dimensions using a volume-of-interest (VOI) atlas. *J Cereb Blood Flow Metab* 1991; **11**:A69–A78.
- [143] Hemler PF, van den Elsen PA, Sumanaweera TS, *et al.* A quantitative comparison of residual error for three different multimodality registration techniques. In: *Proc. Information Processing in Medical Imaging*. Kluwer Academic Publishers, 1995; 251–262.
- [144] Strother SC, Anderson JR, Xu XL, *et al.* Quantitative comparisons of image registration techniques based on high-resolution MRI of the brain. *J Comput Assist Tomogr* 1994; **18**:954–962.
- [145] West J, Fitzpatrick JM, Wang MY, *et al.* Retrospective intermodality registration techniques for images of the head: Surface-based versus volume-based. *IEEE Trans Med Imaging* 1999; **18**:144–150.
- [146] West J, Fitzpatrick JM, Wang MY, *et al.* Comparison and evaluation of retrospective intermodality image registration techniques. *J Comput Assist Tomogr* 1997; **21**:554–566.
- [147] Dean D, Kamath J, Duerk JL, *et al.* Validation of object-induced MR distortion correction for frameless stereotactic neurosurgery. *IEEE Trans Med Imaging* 1998; **17**:810–816.
- [148] Sychra JJ, Pavel DG, Jani A. The accuracy of SPECT brain activation images: Propagation of registration errors. *Med Phys* 1994; **21**:1585–1590.
- [149] Borgefors G. Hierarchical chamfer matching: A parametric edge matching algorithm. *IEEE Trans PAMI* 1988; **10**:849–865.